Use of the Gibbs thermodynamic potential to express the equation of state in atmospheric models

J. Thuburn*

University of Exeter, Exeter, UK

*Correspondence to: Department of Mathematics, College of Engineering, Mathematics and Physical Sciences, University of Exeter, Exeter, EX4 4QF, UK.

The thermodynamics of moist processes is complicated, and in typical atmospheric models numerous approximations are made. However, they are not always made in a self-consistent way, which could lead to spurious sources or sinks of energy and entropy. One way to ensure self-consistency is to derive all thermodynamic quantities from a thermodynamic potential such as the Gibbs function. Approximations may be made to the Gibbs function; these approximations are inherited by all derived quantities in a way that guarantees self-consistency. Here, the feasibility of using the Gibbs function in an atmospheric model is demonstrated through the development of a semi-implicit, semi-Lagrangian vertical slice model, and its application to a standard buoyant bubble test case. The flexibility of the approach is also demonstrated by running the test case with four different equations of state corresponding to dry air, moist air that is saturated, a pseudo-incompressible fluid, and an incompressible fluid. A recently presented 'blended' equation set that unifies the dry fully compressible case and the pseudo-incompressible case is also easily accommodated.

Key Words: Gibbs function; Thermodynamic consistency; pseudo-incompressible; blended equations; physics-dynamics coupling; semi-implicit; SLICE

Received . . .

1. Introduction

In atmospheric models numerous approximations are made in the thermodynamics, particularly where moisture is involved. The approximations are often mutually inconsistent, so that the fundamental laws of thermodynamics are not fully respected. Thermodynamics can be formulated consistently by deriving all thermodynamic quantities from a single thermodynamic potential, such as the Gibbs function, and this approach has been advocated for use in oceanography and ocean modelling (IOC *et al.* 2010), where an accurate equation of state is very complex and has no simple analytical expression. Here the feasibility, as well as flexibility, of using the Gibbs function approach in atmospheric modelling is investigated through the development of a semi-implicit semi-Lagrangian vertical slice model.

At typical atmospheric temperatures and pressures, dry air behaves, to an excellent approximation, as a perfect gas. It obeys a simple equation of state $p = RT\rho$, the specific heat capacities at constant pressure (C_p) and constant volume (C_v) may be taken as constant, and other related thermodynamic quantities such as specific internal energy C_vT, potential temperature $\theta = T(p_0/p)^{R/C_p}$, and specific entropy $\eta = C_p \ln\theta + \text{const}$ have simple analytical expressions. (Standard notation is used for pressure p, temperature T, density ρ, specific gas constant R, and a reference pressure p_0.) For humid air, i.e. a mixture of dry air and water vapour, the situation is only a little more complicated. Again the mixture behaves, to an excellent approximation, as a perfect gas, but now R, C_v and C_p depend on the mass fraction of water q in the mixture.

However, the possibility of condensation and freezing of water considerably complicates the thermodynamics (e.g. Emanuel 1994; Curry and Webster 1999; Feistel *et al.* 2010). Consequently, numerous approximations to the thermodynamics are commonly made in atmospheric models. Examples include assuming the latent heat of vaporization L^v to be constant, using dry air values for R, C_v, C_p, or the ratio $\kappa = R/C_p$, neglecting the volume of liquid water, and neglecting the heat capacity of liquid water. It is far from trivial to ensure that such approximations are made in a self-consistent way so as to respect the laws of thermodynamics and their consequences, and such consistency is not usually enforced. One common example of such an inconsistency is the use of a constant L^v while taking the specific heat capacities of vapour and liquid C_p^v and C^l to be different from each other. Another common example is the use of an accurate empirical formula (such as Bolton 1980) to compute the saturation vapour pressure, while retaining simplifications elsewhere in the thermodynamics so that the Clausius-Clapeyron relation

$$\frac{dp^{\text{sat}}}{dT} = \frac{L^v}{T(\alpha^v - \alpha^l)} \tag{1}$$

(p^{sat} is saturation vapour pressure, α^v and α^l are specific volumes of vapour and liquid) is not exactly satisified. Both of these

examples result in the need for a net (positive or negative) input of energy to take an air parcel around certain reversible thermodynamic cycles in p-T space, violating the first law of thermodynamics, and in a net source or sink of entropy for adiabatic reversible changes involving saturation of water vapour, violating the second law of thermodynamics. Another common source of inconsistency is the use of different approximations in different model components such as the dynamical core and different physical parameterizations. These kinds of inconsistency can result in global energy budget errors of order $1\,\mathrm{Wm}^{-2}$ in a typical weather or climate prediction model (Martin Willett, personal communication 2016).

The issue of thermodynamic consistency also arises when including diabatic heating in approximated equation sets such as the pseudo-incompressible equations (Klein and Pauluis 2012).

One way to ensure that thermodynamics is represented in a self-consistent way in a numerical model is to derive all thermodynamic quantities from a single thermodynamic potential, such as the Gibbs function (e.g. IOC *et al.* 2010; Feistel *et al.* 2010). The Gibbs function is defined by

$$g = e + \alpha p - \eta T \tag{2}$$

where e is specific internal energy and $\alpha = 1/\rho$ is specific volume. It is naturally considered to be a function of pressure, temperature, and composition: $g = g(p, T, q)$. In terms of g, the fundamental thermodynamic relation is

$$dg = -\eta dT + \alpha dp + \mu dq, \tag{3}$$

leading to

$$\alpha = g_p, \qquad \eta = -g_T, \tag{4}$$

where μ is the relative chemical potential of water in air and subscripts on g indicate partial derivatives. When phase changes are possible, consistency requires that equilibrium between phases is determined by equating their temperature, pressure, and chemical potential (e.g. Emanuel 1994; Curry and Webster 1999; Feistel *et al.* 2010). Some other relations between the Gibbs function and commonly used thermodynamic quantities are noted in Appendix A.

Simplifications to the thermodynamics can be made, while maintaining consistency, by approximating the Gibbs function. Section 3 gives some examples. There is a partial analogy here with the use of Hamilton's principle to derive the dynamical equations of motion (Staniforth 2014; Tort and Dubos 2014). The dynamics can be approximated, while maintaining key conservation laws related to dynamical consistency, by approximating the Lagrangian density, provided this is done in a way that preserves its symmetries.

The Gibbs function approach is best implemented in such a way that the Gibbs function and any derivatives needed are evaluated via a single subroutine or function (which may call other subroutines as needed). Having this single interface then greatly facilitates the use of different approximations to the thermodynamics, through the use of different Gibbs functions, within a single model code.

There is growing interest in the design of numerical models with switchable governing equation sets (e.g. Wood *et al.* 2014; Smolarkiewicz *et al.* 2014; Kurowski *et al.* 2014; Benacchio *et al.* 2014; Klein and Benacchio 2016). Of note here is that one widely used approximate equation set, the pseudo-incompressible equation set of Durran (1989), is obtained from the fully compressible equations by modifying only the equation of state, leaving the other governing equations unchanged (see also Klein and Benacchio 2016). It might be hoped, therefore, that the pseudo-incompressible system could be obtained via a suitably specified Gibbs function. In section 3.3 this is confirmed to be the case provided we extend the idea to allow an explicit dependence of g on height z. An incompressible system similar to the Boussinesq equations can be obtained in a similar way. However, some care is needed. For both the pseudo-incompressible and incompressible systems the density is a function only of the entropy (and height), so, given ρ and η, the equation of state does not determine the pressure; the pressure is determined entirely by the dynamical equations. Thus we must use a numerical solution technique that solves the dynamics and the equation of state as a fully coupled system—see section 2.

There are strong benefits from having flexibility in the governing equations while keeping other aspects, such as numerical methods, fixed. It allows commonly made approximations to be relaxed, permitting sensitivity tests to be carried out (Kurowski *et al.* 2014). It could be used to model flows with different composition or variable composition, such as Earth's atmosphere from the ground to the thermosphere (Akmaev 2011), or where the equation of state is not well approximated by a perfect gas, such as the ocean or the deep interior of gas giant planets (e.g. Militzer and Hubbard 2013). It could be used to replace the fully compressible equation of state in a weather forecast model by a pseudo-incompressible equation of state to facilitate comparison with a Large-Eddy model or for acoustic filtering to initialize a compressible integration (Benacchio *et al.* 2014), or by a quasi-incompressible equation of state to facilitate comparison with laboratory flows (e.g. Read *et al.* 2000).

For a general Gibbs function there will not exist explicit expressions for many of the quantities needed to integrate a numerical model or for initialization or diagnostics, so these quantities must be found as solutions of some implicit equations. This apparent complexity might discourage model developers from adopting the approach. Part of the purpose of this paper is to show that any additional complexity, and computational cost, is in fact rather modest. In Appendix A a variety of commonly used quantities are expressed in terms of the Gibbs function.

In principle, any one of the four thermodynamic potentials $e(\alpha, \eta, q)$, $f(\alpha, T, q)$, $g(p, T, q)$, or $h(p, \eta, q)$ (f is the specific Helmholtz function or free energy, h is the specific enthalpy) could be used to derive all the other thermodynamic properties. Section 7 gives some discussion regarding the choice of the Gibbs function.

In this paper it is shown that the Gibbs function representation of thermodynamics can be combined fairly straightforwardly with a typical numerical method for atmospheric dynamics. Section 2 describes the semi-implicit semi-Lagrangian vertical slice model used in this study. The numerical methods are derived from those used in the ENDGame dynamical core (Melvin *et al.* 2010; Wood *et al.* 2014) now operational at the Met Office. The key modification is that the equation of state is everywhere evaluated via a Gibbs function. In particular, in the moist case condensation and evaporation are automatically taken into account as part of the semi-implicit solution procedure, *not* handled in a separate, time-split, physics step as is often done.

Section 3 summarizes the four Gibbs functions that have been implemented so far in the code and used in this study, noting, in particular, the Gibbs functions that give a pseudo-incompressible fluid and an incompressible fluid. Section 4 shows some example results of a standard test case using these four Gibbs functions, demonstrating the flexibility of the Gibbs function approach. Section 5 discusses the errors that can result from handling condensation in a time-split way, and which are avoided in the more tightly coupled scheme presented here. Phase transitions give rise to discontinuous derivatives in some thermodynamic quantities; some possible implications for the numerical solution method are discussed briefly in section 6. Conclusions and further discussion are given in section 7.

2. A semi-implicit semi-Lagrangian scheme using the Gibbs function

For atmospheric modelling it is desirable to enforce mass conservation by solving the density equation in conservative form, and to improve Lagrangian conservation by solving an advection equation for an entropy-like quantity; this is usually taken to be potential temperature or one of its variants; here specific entropy is used. The governing equations are therefore written in the form

$$\frac{D}{Dt}\left(\int_V \rho\, dV\right) = 0, \tag{5}$$
$$\frac{D\eta}{Dt} = 0, \tag{6}$$
$$\frac{Dq}{Dt} = 0, \tag{7}$$
$$\frac{D\mathbf{u}}{Dt} + \frac{1}{\rho}\nabla p + \nabla\Phi = 0, \tag{8}$$
$$1/\rho - g_p(p,T,q) = 0, \tag{9}$$
$$\eta + g_T(p,T,q) = 0. \tag{10}$$

Here Φ is the geopotential, $\mathbf{u} = (u, w)$ is the two-dimensional velocity vector, and D/Dt is the Lagrangian derivative. Coriolis terms are neglected, as are forcing and dissipation terms. This set comprises in effect seven equations for the seven unknowns ρ, η, q, u, w, p, and T.

The numerical methods closely follow those used in ENDGame (Wood *et al.* 2014). Motivated by the desire for good wave dispersion properties, a C-grid staggering is used in the horizontal (u offset half a grid length from ρ) and a Charney-Phillips staggering is used in the vertical (w and η offset by half a grid length from ρ). Second-order centred differences are used to approximate the gradient and divergence. To capture accurately the coupling between moisture and temperature, q is colocated with η. In order to obtain optimal wave dispersion with the $\rho^{-1}\nabla p$ form of the pressure gradient term it is necessary to satisfy the equation of state (i.e. (9) and (10) together) at ρ points

$$\rho = \rho(p, \overline{\eta}, \overline{q}) \tag{11}$$

and also at η points

$$\rho^{(w)} = \rho(\overline{p}, \eta, q), \tag{12}$$

where an overbar indicates a vertical average, in order to determine the density $\rho^{(w)}$ to be used in calculating the vertical component of the pressure gradient term; see Thuburn (2017) for details.

The notation in the density equation (5) indicates that it is integrated using the SLICE scheme of Zerroukat *et al.* (2009), which conservatively transports the mass in a domain-filling set of departure cells to their corresponding arrival cells. The modification of Thuburn *et al.* (2010) is used to ensure accurate departure cell volumes. The code also includes the option to solve the density equation in the form

$$\frac{D\rho}{Dt} + \rho\nabla\cdot\mathbf{u} = 0 \tag{13}$$

using a standard, non-conservative, interpolating semi-Lagrangian scheme. The quantities η, q, and $\mathbf{u}$ are transported using a standard semi-Lagrangian scheme with cubic Lagrange interpolation.

A semi-implicit semi-Lagrangian scheme for this system may then be written

$$[\rho]^{n+1} - [\rho]^n_{\mathrm{SLICE}} = 0, \tag{14}$$
$$[\eta]^{n+1} - [\eta]^n_D = 0, \tag{15}$$
$$[q]^{n+1} - [q]^n_D = 0, \tag{16}$$
$$\left[u + \nu\Delta t\left(\frac{1}{\rho}p_x\right)\right]^{n+1} - \left[u - (1-\nu)\Delta t\left(\frac{1}{\rho}p_x\right)\right]^n_D = 0, \tag{17}$$
$$\left[w + \nu\Delta t\left(\frac{1}{\rho^{(w)}}p_z + \Phi_z\right)\right]^{n+1} - \left[w - (1-\nu)\Delta t\left(\frac{1}{\rho^{(w)}}p_z + \Phi_z\right)\right]^n_D = 0, \tag{18}$$

along with the semi-Lagrangian trajectory departure point calculations for u and w points and (9) and (10) at both ρ and η points. Here, superscripts n and $n+1$ indicate the time step number, subscript D indicates a quantity evaluated at a semi-Lagrangian departure point, and ρ is transported using the SLICE scheme. The off-centring parameter ν is set to $1/2$ giving a centred second-order in time Crank-Nicolson scheme for all the tests described below. Henceforth, to keep the notation compact, details of the spatial discretization are suppressed, except that an overbar indicates where a vertical average is used to transfer a field from ρ points to η points or vice versa, and superscript (w) is used to indicate the density $\rho^{(w)}$ and temperature $T^{(w)}$ that satisfy the equation of state at w points to distinguish them from the density ρ and temperature T that satisfy the equation of state at ρ points. Thus we have a coupled nonlinear system to be solved for the unknowns at timestep $n+1$.

The coupled nonlinear system is solved using an iterative quasi-Newton method. Suppose that after l Newton iterations the right hand sides of (14)-(18) are not necessarily zero but equal to some residuals R_ρ, R_η, R_q, R_u, R_w, while (9) and (10) have residuals $R_{g\rho}$, $R_{g\eta}$ at ρ points and $R^{(w)}_{g\rho}$, $R^{(w)}_{g\eta}$ at w points. We seek increments to the unknowns, indicated by primes, intended to reduce the residuals:

$$\rho' + \nu\Delta t\nabla\cdot\left(\rho^*\mathbf{u}'\right) = -R_\rho, \tag{19}$$
$$\eta' + \nu\Delta t w'\eta^*_z = -R_\eta, \tag{20}$$
$$q' + \nu\Delta t w' q^*_z = -R_q, \tag{21}$$
$$u' + \frac{\nu\Delta t}{\rho^*}p'_x = -R_u, \tag{22}$$
$$w' + \frac{\nu\Delta t}{\rho^*}\left(p'_z - \frac{\rho^{(w)\prime}}{\rho^*}p^*_z\right) = -R_w, \tag{23}$$
$$-\frac{\rho'}{\rho^{*\,2}} - g_{pp}p' - g_{pT}T' - g_{pq}\overline{q'} = -R_{g\rho} \tag{24}$$
$$\overline{\eta'} + g_{pT}p' + g_{TT}T' + g_{Tq}\overline{q'} = -R_{g\eta} \tag{25}$$
$$-\frac{\rho^{(w)\prime}}{\rho^{*\,2}} - g_{pp}\overline{p'} - g_{pT}T^{(w)\prime} - g_{pq}q' = -R^{(w)}_{g\rho} \tag{26}$$
$$\eta' + g_{pT}\overline{p'} + g_{TT}T^{(w)\prime} + g_{Tq}q' = -R^{(w)}_{g\eta}. \tag{27}$$

The left hand sides of (19)-(27) are an approximate linearization of (14)-(18) and the equation of state about a reference state indicated by asterisks. (The derivatives of g on the left hand side are also evaluated at the reference state.) There is some freedom in the choice of the reference state, but it should be close to the actual state for rapid convergence of the Newton iterations. Here the reference state is taken to be the solution at time step n.

Although the linear system (19)-(27) appears somewhat daunting, systematic elimination of unknowns leads to a

familiar Helmholtz problem (or Poisson-like problem in the incompressible or pseudo-incompressible cases). Elimination of $T^{(w)\prime}$ from (26), (27) gives

$$-\frac{\rho^{(w)\prime}}{\rho^{*\,2}} + \left(\frac{g_{pT}^2}{g_{TT}} - g_{pp}\right)\overline{p'} + \left(\frac{g_{pT}}{g_{TT}}\right)\eta' + \left(\frac{g_{pT}g_{Tq}}{g_{TT}} - g_{pq}\right)q' = -R_{g\rho}^{(w)} - \frac{g_{pT}}{g_{TT}}R_{g\eta}^{(w)}, \quad (28)$$

or*

$$-\frac{\rho^{(w)\prime}}{\rho^*} + (\ln\rho)_p^*\Big|_{\eta q}\overline{p'} + (\ln\rho)_\eta^*\Big|_{pq}\eta' + (\ln\rho)_q^*\Big|_{\eta p}q' = -\rho^* R_{g\rho}^{(w)} - (\ln\rho)_\eta^*\Big|_{pq}R_{g\eta}^{(w)}. \quad (29)$$

(Subscripts to the right of the vertical bars indicate what is held constant when the partial derivatives are taken.) Using (20) and (21) to eliminate η' and q', applying the definition of the reference state sound speed c

$$(\ln\rho)_p^*\Big|_{\eta q} = \frac{1}{\rho^* c^2}, \quad (30)$$

and defining N^2 by

$$N^2 = \left((\ln\rho)_\eta^*\Big|_{pq}\eta_z^* + (\ln\rho)_q^*\Big|_{\eta p}q_z^*\right)\frac{p_z^*}{\rho^*}, \quad (31)$$

(29) becomes

$$-\frac{\rho^{(w)\prime}}{\rho^*} + \frac{\overline{p'}}{\rho^* c^2} - \nu\Delta t\frac{\rho^* N^2}{p_z^*}w' = R_{\rm eos}^{(w)}, \quad (32)$$

where

$$R_{\rm eos}^{(w)} = -\rho^* R_{g\rho}^{(w)} + (\ln\rho)_\eta^*\Big|_{pq}\left(R_\eta - R_{g\eta}^{(w)}\right) + (\ln\rho)_q^*\Big|_{\eta p}R_q. \quad (33)$$

Eliminating $\rho^{(w)\prime}/\rho^*$ from (23) then leaves

$$\left(1+\nu^2\Delta t^2 N^2\right)w' + \frac{\nu\Delta t}{\rho^*}\left(p_z' - \frac{p_z^*}{\rho^* c^2}\overline{p'}\right) = -R_w - \frac{\nu\Delta t p_z^*}{\rho^*}R_{\rm eos}^{(w)}. \quad (34)$$

Defining the vertical derivative operator

$$\mathcal{D}_1(p') \equiv \frac{1}{(1+\nu^2\Delta t^2 N^2)}\left(p_z' - \frac{p_z^*}{\rho^* c^2}\overline{p'}\right) \quad (35)$$

allows (34) to be written compactly as

$$w' + \frac{\nu\Delta t}{\rho^*}\mathcal{D}_1(p') = R_{pw}, \quad (36)$$

where

$$R_{pw} = \frac{-1}{(1+\nu^2\Delta t^2 N^2)}\left(R_w + \frac{\nu\Delta t p_z^*}{\rho^*}R_{\rm eos}^{(w)}\right). \quad (37)$$

Next, the analogue of (32) at ρ points is

$$-\frac{\rho'}{\rho^*} + \frac{p'}{\rho^* c^2} - \nu\Delta t\frac{N^2}{p_z^*}\overline{\rho^* w'} = R_{\rm eos}, \quad (38)$$

where

$$R_{\rm eos} = -\rho^* R_{g\rho} + (\ln\rho)_\eta^*\Big|_{pq}\left(\overline{R_\eta} - R_{g\eta}\right) + (\ln\rho)_q^*\Big|_{\eta p}\overline{R_q}. \quad (39)$$

Using (38) to eliminate ρ' from (19) gives

$$\frac{p'}{c^2} + \nu\Delta t\left(\rho^* u'\right)_x + \nu\Delta t\mathcal{D}_2\left(\rho^* w\right) = -R_\rho + \rho^* R_{\rm eos}, \quad (40)$$

where

$$\mathcal{D}_2\left(\rho^* w'\right) \equiv \left(\rho^* w'\right)_z - \frac{\rho^*}{p_z^*}N^2\overline{\rho^* w'}. \quad (41)$$

Finally, using (22) and (36) to eliminate u' and w' from (40) leaves

$$\frac{p'}{c^2} - \nu^2\Delta t^2\left\{p'_{x\,x} + \mathcal{D}_2\mathcal{D}_1(p')\right\} = R_H, \quad (42)$$

where

$$R_H = -R_\rho + \rho^* R_{\rm eos} + \nu\Delta t\left(\rho^* R_u\right)_x - \nu\Delta t\mathcal{D}_2\left(\rho^* R_{pw}\right). \quad (43)$$

Equation (42) is a typical Helmholtz problem that arises from implicit or semi-implicit integration of compressible fluid equations. A variety of methods are available for its solution; here a horizontally-multigrid method is used with a vertical line solve and an underrelaxed Jacobi smoother in the horizontal. A single V-cycle gives sufficient accuracy for rapid convergence of the Newton iterations, except for the incompressible and pseudo-incompressible cases for which two V-cycles are needed to avoid noise in the divergence field. Having found p', the increments to other variables are found by back-substitution, and the Newton update is carried out on all variables. Three Newton iterations were used for the results shown below.

Note that the coefficients of the Helmholtz problem depend on the equation of state only through the terms N^2 and $1/c^2$. In the moist case these quantities are defined in such a way that they automatically take into account the effects of condensation and evaporation. In the incompressible and pseudo-incompressible cases $1/c^2$ goes to zero (section 3.3) and the Helmholtz problem becomes a less local Poisson-like problem.

The Helmholtz problem (42) is only guaranteed to have a solution if the Helmholtz operator on the left hand side is elliptic. As with any model that treats gravity waves implicitly, this property can break down if the coefficient $\left(1+\nu^2\Delta t^2 N^2\right)$ in (35) becomes negative, which could happen if N^2 becomes negative and Δt is too large. The inclusion of condensation effects in the calculation of N^2 might make the occurrence of negative N^2 more likely. It is common practice in numerical models (e.g. Davies *et al.* 2005) to limit the values of N^2 used in this coefficient to prevent loss of ellipticity. Such a measure is not needed in the experiments discussed below because of the relatively small time steps used; however, it would be needed in a larger-scale model taking longer time steps.

3. Some example Gibbs functions

Feistel *et al.* (2010) provide a very accurate expression, as a set of functional fits to the best available experimental data, for the Helmholtz function of humid air, from which the Gibbs function may be calculated. It provides a valuable benchmark, but is more accurate, and more complex, than needed for most meteorological modelling. This section presents some example Gibbs functions that might be used in meteorological models, for dry air and wet air, and also for a pseudo-incompressible fluid and an incompressible fluid. (But note that, for weather forecasting or climate modelling, an extension to include ice would be a minimum requirement.)

* Using the standard formula for change of independent variable in a partial derivative, e.g. $\alpha_p|_\eta = \alpha_p|_T + \alpha_T\big|_p T_p|_\eta$.

Many quantities of physical interest are given by or involve the first and second derivatives of g. The derivatives are also needed if a Newton method is used to solve the implicit equations that give other quantities of interest (Appendix A). The first and second derivatives of g for each of the examples below are given in Appendix B.

3.1. *Dry air*

One simple example of a Gibbs function suitable for idealized modelling is that of dry air approximated as a perfect gas:

$$g(p,T) = -C_p^d T \ln\left(\frac{T}{T_0}\right) + R^d T \ln\left(\frac{p}{p_0^d}\right). \tag{44}$$

Here R^d and C_p^d are constants, superscripts d indicate dry air values, and T_0 and p_0^d are constant reference values. The values of all constants used are summarized in Table 1.

Note we have some freedom in the specification of g; we can add $A + BT$ for arbitrary constants A and B. The effect of A is to offset the origin of g or equivalently e, by a constant. The effect of B is to offset the origin of η by a constant. In both cases there is no effect on any quantity that can be measured by physical experiment.

3.2. *Humid and wet air*

Humid air, a mixture of dry air and water vapour without liquid water, can be treated, to an excellent approximation, as a mixture of perfect gases (Feistel *et al.* 2010). Let a be the mass fraction of dry air in the mixture. Then

$$g^{av}(p,T,a) = a g^a + (1-a) g^v \tag{45}$$

where

$$g^a(p^d,T) = -C_p^d T \ln\left(\frac{T}{T_0}\right) + R^d T L^{(1)} \tag{46}$$

and

$$g^v(p^v,T) = -C_p^v T \ln\left(\frac{T}{T_0}\right) + R^v T L^{(2)} + L_0^v\left(1 - \frac{T}{T_0}\right). \tag{47}$$

Here superscript v indicates values related to water vapour, L_0^v is a constant,

$$L^{(1)} = \ln\left(\frac{p^d}{p_0^d}\right) = \ln\left(\frac{\varepsilon a p}{(1+a(\varepsilon-1))\,p_0^d}\right), \tag{48}$$

$$L^{(2)} = \ln\left(\frac{p^v}{p_0^v}\right) = \ln\left(\frac{(1-a)p}{(1+a(\varepsilon-1))\,p_0^v}\right), \tag{49}$$

$\varepsilon = R^d/R^v$, and p_0^v is another constant. As noted above, we are free to add the last term on the right hand side in (47); it will be used below to ensure consistency with the liquid water Gibbs function. (We follow Feistel *et al.* (2010), who express g^{av} as a function of the mass fraction of dry air a rather than the mass fraction of water vapour because this leads to a formal symmetry between humid air and saline water.)

If we treat liquid water as an incompressible fluid of constant density then its Gibbs function may be written (e.g. Vallis 2006, with his β parameters set to zero and specific choices for other constants)

$$g^l(p,T) = -C^l T \ln\left(\frac{T}{T_0}\right) + \alpha^l\left(p - p_0^{\rm sat}\frac{T}{T_0}\right). \tag{50}$$

Here superscript l indicates values related to liquid water, α^l is the constant specific volume of liquid water and $p_0^{\rm sat}$ is another constant that will turn out to equal the saturation vapour pressure of pure water vapour at $T = T_0$.

The total Gibbs function for moist air, possibly containing liquid water, is then given by

$$g(p,T,q) = (1-q^l) g^{av}(p,T,a) + q^l g^l(p,T), \tag{51}$$

where q is the mass fraction of total water in the sample, q^l is the mass fraction of liquid water in the sample, and $a = (1-q)/(1-q^l)$ is the mass fraction of dry air *in the gaseous part of the sample*.

To complete the calculation it remains to determine a and q^l from the requirement that either the liquid water and water vapour should be in equilibrium or there should be no liquid water. For equilibrium the liquid water and water vapour should have the same pressure, temperature, and chemical potential (e.g. Feistel *et al.* 2010). Since the pressure and temperature are input arguments to the Gibbs function, the first two conditions are automatically satisfied. The chemical potential of water vapour in the air-vapour mixture is given by

$$\mu^v(p,T,a) = g^{av} - a g_a^{av} \tag{52}$$

(Feistel *et al.* 2010). For the g^{av} given above, which neglects certain virial interaction terms between water vapour and air, it may be verified that

$$\mu^v = g^v(p^v,T), \tag{53}$$

which is assumed in much of the literature on atmospheric thermodynamics (e.g. Emanuel 1994; Curry and Webster 1999). (However, the code described here implements the full version (52) in readiness for more general g^{av}.) In the absence of salinity etc., the chemical potential of liquid water is given simply by its Gibbs function

$$\mu^l(p,T) = g^l. \tag{54}$$

A practical way to complete the calculation is to determine the saturation value of a, given p and T, by solving

$$\mu^v(p,T,a_{\rm sat}) = \mu^l(p,T). \tag{55}$$

Given a good first guess for $a_{\rm sat}$, for example by using a standard approximation for the saturation vapour pressure $p^{\rm sat}$ followed by

$$a_{\rm sat} = \frac{p - p^{\rm sat}}{p + (\varepsilon-1)p^{\rm sat}}, \tag{56}$$

a single Newton iteration is found to give a sufficiently accurate solution. If $q < 1 - a_{\rm sat}$ then there is insufficient water to achieve saturation, so we have $q^l = 0$, $q^v = q$, $a = 1-q$, and

$$g(p,T,q) = g^{av}(p,T,a). \tag{57}$$

If $q \geq 1 - a_{\rm sat}$ then there is sufficient water to achieve saturation, so $a = a_{\rm sat}$, $q^l = (q + a - 1)/a$, and $q^v = q - q^l$, and the Gibbs function is given by (51).

As noted above, there is some freedom in the choice of certain constants in the Gibbs functions g^a, g^v, g^l. However, these must be chosen consistently between vapour and liquid in order to give the correct latent heat of vaporization and saturation vapour pressure. The latent heat of vaporization is given by (74), which, for the equation of state discussed here, reduces to

$$L^v = h^v - h^l \tag{58}$$

where

$$h^v = g^v + \eta^v T = C_p^v T + L_0^v \tag{59}$$

and

$$h^l = g^l + \eta^l T = C^l T + \alpha^l p \tag{60}$$

are the specific enthalpies of vapour and liquid respectively, evaluated using (47) and (50). Thus

$$L^v = L_0^v + \left(C_p^v - C^l\right) T - \alpha^l p, \tag{61}$$

so the constant L_0^v must be chosen to be the latent heat of vaporization extrapolated to $T = 0$ and $p = 0$. Also, the condition for equilibrium between vapour and liquid (55) here reduces to $g^v = g^l$. Substituting from (47) and (50) and evaluating at $T = T_0$ with $p = p^v = p_0^{\rm sat}$ gives

$$R^v T_0 \ln\left(\frac{p_0^{\rm sat}}{p_0^v}\right) = 0. \tag{62}$$

This is satisfied provided we choose $p_0^v = p_0^{\rm sat}$.

3.3. *Pseudo-incompressible fluid*

The pseudo-incompressible system of Durran (1989) has an equation of state of the form

$$\rho\theta = \rho_r(z)\theta_r(z) = \frac{p_0^d}{R^d}\left(\frac{p_r(z)}{p_0^d}\right)^{1-\kappa} \tag{63}$$

where ρ_r, θ_r and p_r are reference profiles that are functions only of height. By integrating and making some specific choices for functions of integration (details omitted) we obtain a Gibbs function that has a form somewhat reminiscent of the dry air Gibbs function (44):

$$g(p,T,z) = C_p^d T\left[\ln\left\{\Pi_r\left((1-\kappa) + \kappa\frac{p}{p_r}\right)\right\} - \ln\left(\frac{T}{T_0}\right)\right], \tag{64}$$

where $\Pi_r(z) = \left(p_r/p_0^d\right)^\kappa$ is the reference Exner function profile.

It may be verified that the internal energy density $\rho e = \rho(g + \eta T - \alpha p)$ agrees with the expression $C_v^d \rho_r \Pi_r \theta_r$ given by Durran (1989). It may also be verified that the form of N^2 defined in (31) remains appropriate despite the explicit z dependence in g. By construction, this Gibbs function gives

$$\frac{1}{c^2} = \left.\frac{\partial\rho}{\partial p}\right|_\eta = \frac{g_{pT}^2 - g_{pp}g_{TT}}{g_p^2 g_{TT}} = 0. \tag{65}$$

Thus the first term on the left hand side of (42) vanishes.

3.4. *Incompressible fluid*

A special case of the pseudo-incompressible system is obtained by setting $\rho_r(z)\theta_r(z) = p_0^d/R^d = \text{const}$, $p_r = p_0^d$, $\Pi_r = 1$:

$$g(p,T) = C_p^d T\left[\ln\left((1-\kappa) + \kappa\frac{p}{p_0^d}\right) - \ln\left(\frac{T}{T_0}\right)\right]. \tag{66}$$

In this case the density is a function only of the potential temperature, so if $D\theta/Dt = 0$ then $D\rho/Dt = 0$ and $\nabla\cdot\mathbf{u} = 0$.

For both the pseudo-incompressible and incompressible cases, a variety of different Gibbs functions are possible that give the desired equation of state. The forms given here have been chosen so that parameters such as p, T, and θ retain more or less intuitive interpretations comparable with the compressible case. But note the slightly modified interpretation of θ in the pseudo-incompressible case: it is the temperature that an air parcel would have if moved reversibly and adiabatically to the reference pressure p_0^d *and height* $z = 0$.

4. Example results

The flexibility of the Gibbs function approach is demonstrated using the standard buoyant bubble test case of Bryan and Fritsch (2002). For a dry air case and for a saturated moist air case, Bryan and Fritsch (2002) impose an identical initial positive buoyancy perturbation upon a resting, neutrally stratified, hydrostatically balanced background state and follow the subsequent evolution over a time of 1000 s.

In the dry case the constant background potential temperature is set to $\theta_0 = 300\,\text{K}$ and the buoyancy is given by $\Phi_z\theta'/\theta_0$ where θ' is the potential temperature perturbation. (Although not stated explicitly, Bryan and Fritsch appear to hold the pressure fixed as they perturb buoyancy, and we do the same here.) In the saturated case the total water mixing ratio is $r = q/(1-q) = 0.02$, the constant background equivalent potential temperature is set to $\theta_{e\,0} = 320\,\text{K}$, and the buoyancy is expressed in terms of a buoyancy potential temperature. An equivalent definition of buoyancy in both cases (assuming zero pressure perturbation) is $-\Phi_z\rho'/\rho$ (note the denominator is the full ρ, not the background value) and this definition generalizes to arbitrary equations of state, so it is used here for all cases. Provided we use the same values of all physical constants (Table 1) and set α^l to zero, the Gibbs function (44) gives the Bryan and Fritsch dry case and the Gibbs function (51) gives the Bryan and Fritsch saturated case.

In addition to the two Bryan and Fritsch cases, two further, analogous, cases were carried out. The first used the pseudo-incompressible Gibbs function (64), taking the reference profile to be the hydrostatically balanced background profile $\Pi_r = 1 - \Phi/(C_p^d\theta_0)$ and $p_r = p_0^d\Pi_r^{1/\kappa}$, with background potential temperature $\theta_0 = 300\,\text{K}$. The second used the incompressible Gibbs function (66) with background potential temperature $\theta_0 = 375\,\text{K}$. In all cases the surface pressure was set to $10^5\,\text{Pa}$.

As in Bryan and Fritsch (2002), a 20 km wide and 10 km deep domain is used with the initial buoyant perturbation centred at $x = 10\,\text{km}$, $z = 2\,\text{km}$. The results shown here use 192×96 grid cells, which is convenient for the multigrid solver, giving a slightly coarser resolution than the 100 m used by Bryan and Fritsch (2002). The time step was set to $\Delta t = 10\,\text{s}$.

Figure 1 shows the potential temperature perturbation and Fig. 2 shows the vertical velocity for the four cases at $t = 1000\,\text{s}$. The dry air and saturated cases agree very closely with the benchmark simulations of Bryan and Fritsch (2002). The solution in the pseudo-incompressible case is almost identical to the compressible dry air case, in agreement with Benacchio *et al.* (2014). In the absence of numerical errors and neglecting pressure fluctuations, the buoyancy would be materially conserved in the three dry cases; in fact the peak decreases by around $10-15\%$ (not shown) due to numerical errors. In the saturated case, on the other hand, latent heating generates additional buoyancy (the peak value increases by about 38%); consequently the bubble in the saturated case rises slightly faster and grows slightly bigger than in the dry compressible and pseudo-incompressible cases. The bubble in the incompressible case conserves its initial volume and so remains smaller than the other three, which expand as they rise.

As another example of the flexibility of the approach, the sensitivity to the specific volume of liquid water was tested by changing α^l from zero to the more realistic value $10^{-3}\,\text{m}^3\text{kg}^{-1}$. In fact the sensitivity is extremely small: the maximum w at $t = 1000\,\text{s}$ increased by only about $0.5\,\text{mm}\,\text{s}^{-1}$ compared to the result shown in Fig. 2(b). But the point is that such a sensitivity test would be quite difficult to carry out with the usual approach to atmospheric model thermodynamics because there is no longer a (consistent) explicit analytical expression for the saturation vapour pressure, whereas in the present approach it is a simple matter of changing one model parameter.

Table 1. Constants used for the results shown in section 4

Constant	Description	Value
C_p^d	Specific heat capacity of dry air at constant pressure	$1004\,\mathrm{Jkg^{-1}K^{-1}}$
C_p^v	Specific heat capacity of water vapour at constant pressure	$1885\,\mathrm{Jkg^{-1}K^{-1}}$
C^l	Specific heat capacity of liquid water at constant pressure	$4186\,\mathrm{Jkg^{-1}K^{-1}}$
L_0^v	Latent heat of vaporization at $T=0$, $p=0$	$3.1285\times10^6\,\mathrm{Jkg^{-1}}$
p_0^d	Reference pressure for dry air	$10^5\,\mathrm{Pa}$
p_0^v	Reference pressure for water vapour	$p_0^v = p_0^{\mathrm{sat}}$
p_0^{sat}	Saturation vapour pressure for pure water at $T=T_0$	$611.2\,\mathrm{Pa}$
R^d	Gas constant for dry air	$287\,\mathrm{Jkg^{-1}K^{-1}}$
R^v	Gas constant for water vapour	$461\,\mathrm{Jkg^{-1}K^{-1}}$
T_0	Reference temperature	$273.15\,\mathrm{K}$
α^l	Specific volume of liquid water	$0\,\mathrm{m^3kg^{-1}}$
ε	Ratio of R^d and R^v	$\varepsilon = R^d/R^v$
κ	Ratio of R^d and C_p^d	$\kappa = R^d/C_p^d$

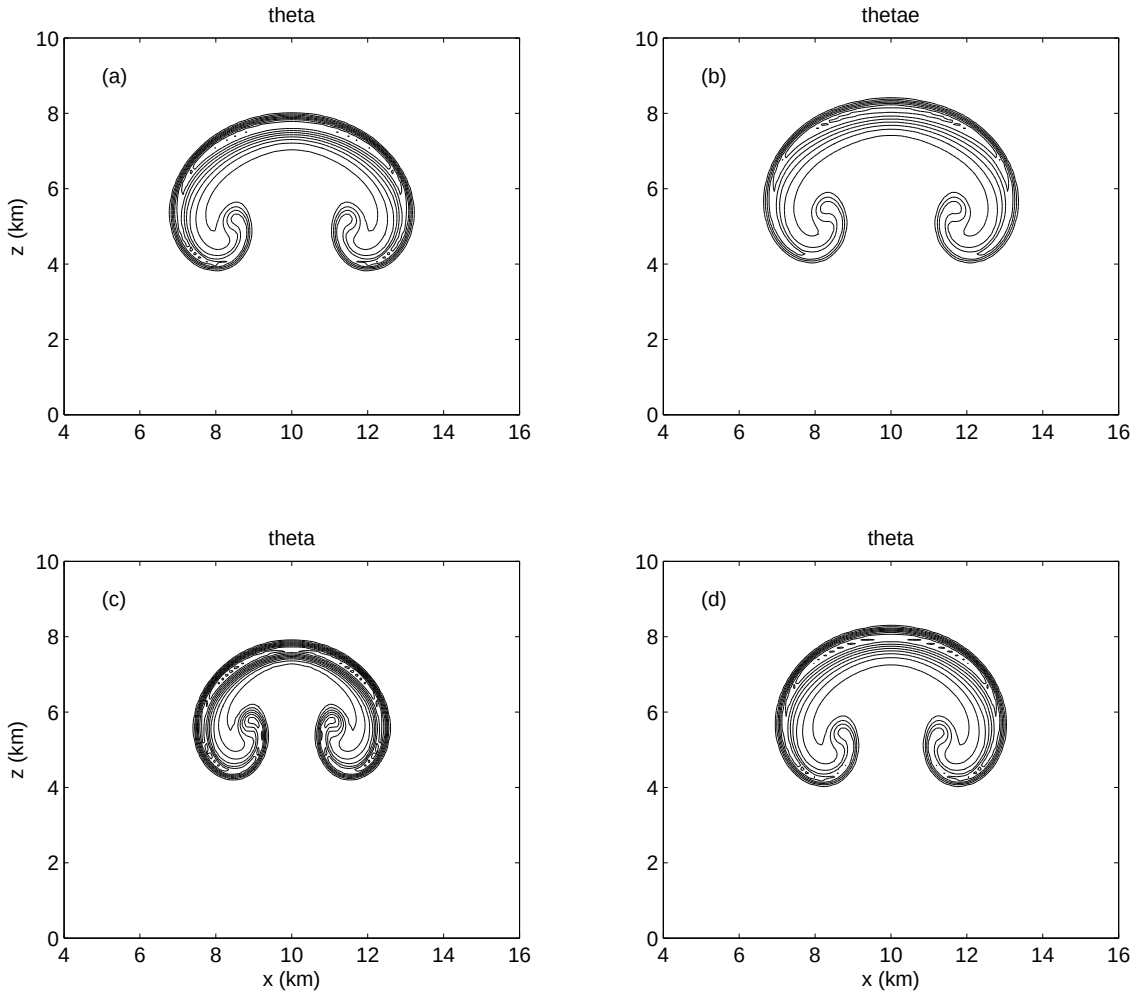

Figure 1. Perturbation to potential temperature or equivalent potential temperature (K) at $t = 1000\,\mathrm{s}$ for (a) dry air, (b) saturated air, (c) incompressible fluid, (d) pseudo-incompressible fluid. The contour interval is $0.2\,\mathrm{K}$ except in (b) where it is $0.5\,\mathrm{K}$.

5. Physics-dynamics coupling

In many atmospheric models the time stepping is split. First the increments due to dynamics and transport are computed and added, then the increments due to other physical processes, including an adjustment back to saturation in any air that has become supersaturated as a result of dynamics and transport. To get an estimate of the magnitude of the errors that result from such splitting the following simple calculation was carried out. An air parcel was assumed to have initial pressure $p = 10^5\,\mathrm{Pa}$, temperature $T = 280\,\mathrm{K}$, and specific humidity $q = 0.00196$. The parcel was then 'lifted' in such a way as to mimic a split time stepping scheme. The parcel's pressure was reduced by an amount corresponding to an ascent of $100\,\mathrm{m}$, and the temperature computed so as to maintain the total entropy of the parcel *while keeping q^v and q^l fixed*. Then, if the parcel was supersaturated,

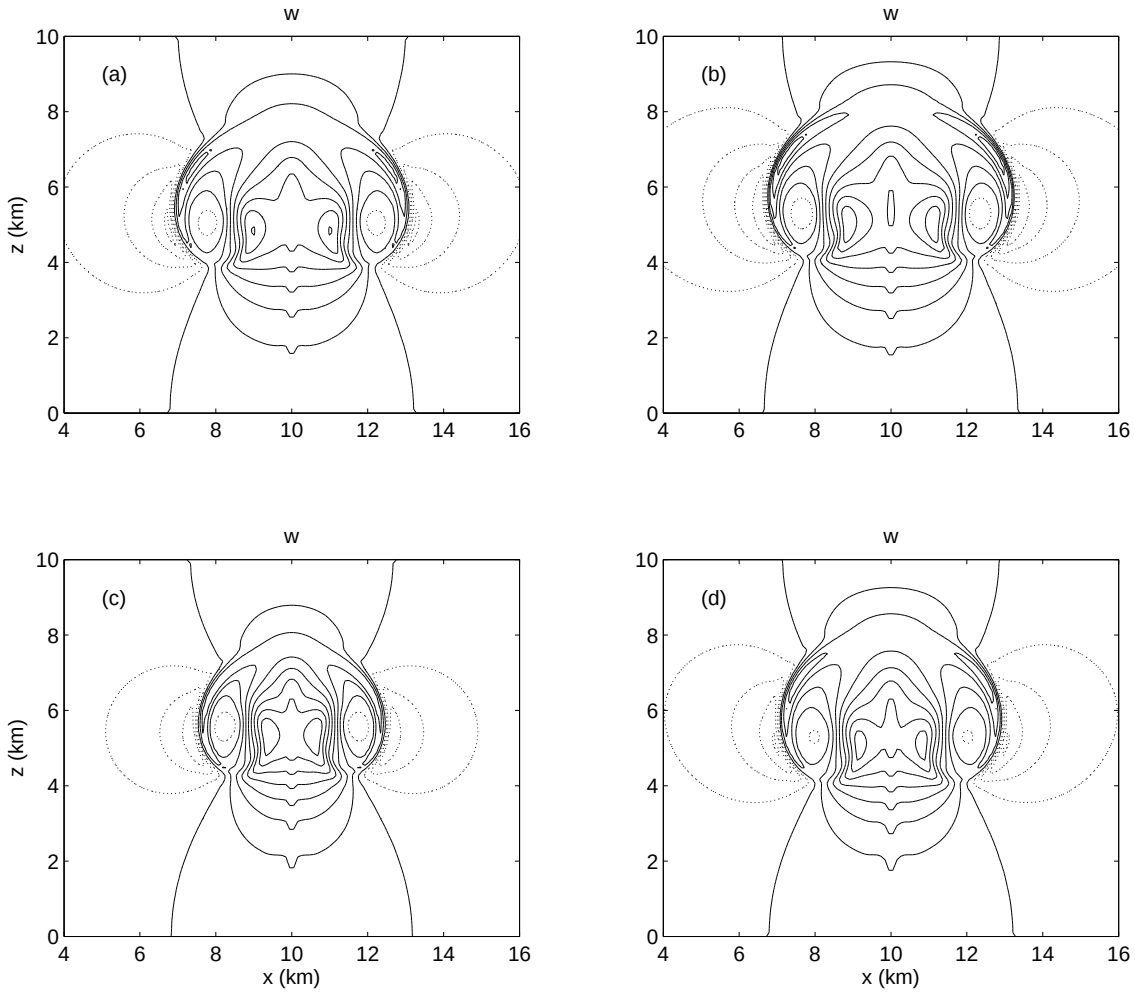

Figure 2. Vertical velocity (ms^{-1}) at $t = 1000\,\mathrm{s}$ for (a) dry air, (b) saturated air, (c) incompressible fluid, (d) pseudo-incompressible fluid. Contour interval is $2\,\mathrm{ms}^{-1}$.

it was adjusted back to saturation while conserving its volume and total internal energy. One hundred such step were carried out, lifting the parcel to a height of $10\,\mathrm{km}$. This parcel was compared with a control parcel that conserved entropy and was allowed to adjust to saturation as it was lifted.

Figure 3 shows the results of this calculation. As expected, the two parcels are identical until the height at which condensation begins, close to $2\,\mathrm{km}$. Above this height, the time split parcel has slightly less buoyancy than the control parcel. This happens because, at the end of the first part of the split step, not all of the latent heat has been released to produce buoyancy. At the end of the saturation adjustment the latent heat has been released, but since this occurs at constant volume the buoyancy has still not been realized. Thus the buoyancy of the time split parcel effectively lags one step behind the control parcel.

In the time split calculation the parcel becomes supersaturated before condensation occurs; thus there should be a net production of entropy because the condensation occurs irreversibly. This entropy production is visible as an increase in θ_e. The increase is, in fact, very small, of order $0.01\,\mathrm{K}$, but it is systematic and measurable.

The release of latent heat during the second part of the split step increases the pressure of the parcel. If the dynamics and transport step produced a parcel pressure in balance with its surroundings then this latent-heat-induced perturbation will be unbalanced, and in a full model could manifest as spurious acoustic waves. Figure 3 shows this pressure perturbation peaking at around $0.75\,\mathrm{hPa}$, which is comparable to the pressure perturbations seen in the compressible buoyant bubble case of section 4 (not shown). Thus, although the buoyancy errors and entropy errors resulting from time splitting are both very small, in fact much smaller than those resulting from advection errors, the pressure errors are significant. For this reason, Bryan and Fritsch (2002) use an unsplit time integration scheme that includes condensation terms along with the dynamics and transport, and they iterate the time step in order to obtain a condensation rate that prevents supersaturation at the end of the time step. In this way, their time integration scheme behaves like the control parcel in the calculation of Fig. 3. In the model described here, the same effect is achieved by building the assumption of no supersaturation into the Gibbs function, and coupling the full, moist equation of state to the dynamics through the semi-implicit time integration scheme.

Another advantage of the approach used here is that the quantity N^2 appearing in the Helmholtz problem is the full static stability experienced by the fluid, taking into account any condensation or evaporation. This will help to ensure good convergence of the fully coupled Newton solver of section 2.

6. Numerical effects near phase transitions

For initializing the model, for the time integration itself, and for calculating diagnostics for output, there are many places where it is necessary to compute some thermodynamic quantity from those that are already known. This can either be done directly

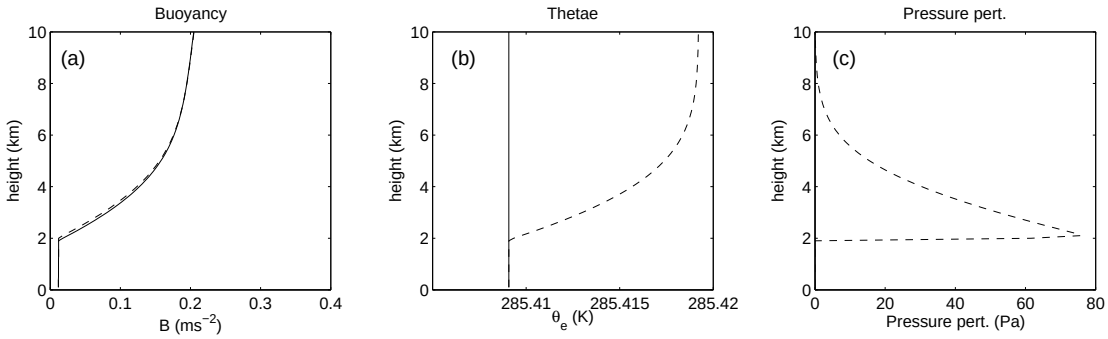

Figure 3. (a) Buoyancy (ms^{-2}), (b) Equivalent potential temperature (K), (c) Pressure perturbation (Pa), for a rising air parcel computed using a split time step (dashed) and a control air parcel (solid).

or through some iterative calculation such as the Newton method (Appendix A). However, a caveat should be given. Near phase transitions some quantities have discontinuous derivatives, so a Newton method might converge slowly or even fail to converge. In fact, the only example of such a calculation encountered by the author for which a Newton iteration fails to converge is in calculating T given p, q, and enthalpy h:

$$g(p,T,q) - Tg_T(p,T,q) = h. \tag{67}$$

A practical solution for this example is first to determine the dewpoint temperature T_d (83) (Appendix A) and hence dewpoint enthalpy h_d, and then use either the unsaturated Gibbs function or the saturated Gibbs function according to whether $h \le h_d$ or $h > h_d$, thus avoiding the discontinuous derivative $h_T|_{pq}$.

Another potential issue that might arise near phase transitions is that N^2 defined by (31) will be discontinuous between unsaturated air and adjacent saturated air. The resulting roughness in the Helmholtz coefficients might adversely affect convergence of the solver.

These issues do not affect the test cases described above because the air is either always dry or always saturated. Therefore, to investigate these effects a further test case was carried out. The full moist air equation of state (51) was used. The initial buoyancy perturbation was identical to the other four test cases, but the initial specific humidity was set to either $0.002/1.02$ (one tenth of the value in the saturated test case) or 95% of the saturation value, whichever is smaller. Initially there is no liquid water, but as the buoyant bubble rises the air within becomes saturated and a cloud forms, so that saturated and subsaturated regions co-exist. Examination of the N^2 field for the dry case, the saturated case, and this cloud case shows that it is dominated by the sharp gradients in θ or θ_e that form at the edge of the rising bubble due to transport and shear; the cloud case is not noticeably more rough than the other two. The convergence of the solver was also investigated by looking at the residuals in (19)-(27) and (43). and how they decreased with iteration number. Again there was no noticeable difference between the cloud case and the dry and saturated cases. The maximum residuals typically decrease by an order of magnitude per iteration in all three cases.

Thus, for the test cases investigated here, numerical effects near phase transitions have no adverse effect on the solution method. However, it is important to be aware of the possibility of such effects in other situations.

7. Conclusions and Discussion

The feasibility of specifying the equation of state via the Gibbs thermodynamic potential within a semi-implicit semi-Lagrangian flow solver has been demonstrated. The flexibility of the approach has been shown by carrying out a standard buoyant bubble test case using four different equations of state: dry air, saturated air, incompressible fluid, and pseudo-incompressible fluid. In the pseudo-incompressible case the Gibbs function must be allowed an explicit dependence on z as well as on p, T and q. In the incompressible and pseudo-incompressible cases, the equation of state, given ρ and η, does not determine the pressure. Thus the equation of state and the dynamical equations arising from the implicit time integration must be solved as a single coupled system. This is analogous to the inclusion of a hydrostatic switch in the ENDGame solver (Wood *et al.* 2014); it is only straightforward for an implicit time integration scheme.

'Blended' equation sets (e.g. Benacchio *et al.* 2014; Klein and Benacchio 2016), for example an equation set intermediate between compressible dry air and pseudo-incompressible, can be obtained by combining the corresponding Gibbs functions in appropriate ways. Thermodynamic consistency is automatically guaranteed by the approach. It may be verified that the particular blended compressible-pseudo-incompressible equation set of Klein and Benacchio (2016) is given not by a simple weighted average of (44) and (64), but by

$$\begin{aligned} g(p,T) &= C_p^d T \left[\ln\left\{ \beta\Pi + (1-\beta)\Pi_r \left((1-\kappa) + \kappa \frac{p}{p_r} \right) \right\} \right. \\ &- \left. \ln\left(\frac{T}{T_0} \right) \right], \end{aligned} \tag{68}$$

where $\beta \in [0,1]$ is the blending parameter (called α in Klein and Benacchio 2016), with $\beta = 0$ giving pseudo-incompressible and $\beta = 1$ giving fully compressible.

It is worth commenting that the incompressible system studied here is not equivalent to the Boussinesq equations. Unlike the Boussinesq equations, the full density is used wherever density appears. Density is a function only of entropy, independent of pressure; thus $1/c^2 = 0$ and, in the absence of diabatic heating, density is materially conserved and the divergence vanishes. However, diabatic heating can modify the entropy and hence the density of an air parcel, so a non-zero divergence is needed to accommodate the change in specific volume. In the Boussinesq equations, on the other hand, it is volume rather than mass that is conserved, and zero divergence is enforced even under diabatic heating. The numerical methods used here respect the mass budget exactly. Thus, any Lagrangian changes in density, including heating-induced changes in the incompressible case, are accompanied by a corresponding divergence. When explicit diabatic heating is absent in the incompressible case, as in section 4 above, zero divergence is not directly enforced by the numerics, but it is hoped that the solver will indeed give divergence close to zero. Figure 4 shows the divergence at $t = 1000\,\mathrm{s}$ for the incompressible case and, for comparison, the dry compressible case. In the compressible case the divergence is very strongly correlated with the vertical velocity (Fig. 2), as expected. In the incompressible case the peak divergence is

two orders of magnitude smaller, and the non-zero values are concentrated around the sharp entropy gradients at the edge of the bubble. These are the locations where the numerical errors in the advection of η and ρ, the fact that η and ρ use different advection schemes, and the averaging of η to ρ points because of the vertical grid staggering will have greatest effect. The importance of accurate mass conservation is shown by one further test. When the incompressible experiment is repeated with standard interpolating semi-Lagrangian advection of ρ rather than SLICE, the spurious divergence is an order of magnitude larger.

On a related point, the model code, as currently formulated, conserves the total density, but not necessarily the dry mass and water that make up that total. Since the sources and sinks of dry mass are essentially zero even when there are strong sources and sinks of water, it might be desirable to conserve dry mass exactly. This could be achieved straightforwardly by replacing (14) by the corresponding equation for dry mass

$$\left[\rho^d\right]^{n+1} - \left[\rho^d\right]^n_{\text{SLICE}} = 0, \tag{69}$$

and diagnosing $\rho = (1+\bar{q})\rho^d$ as needed.

By coupling the full equation of state to the dynamics via the Gibbs function, including the equilibrium between water vapour and liquid in the saturated case, the numerical integration scheme presented here prevents the occurrence of supersaturation, and eliminates the unbalanced pressure perturbations that could result from a time split treatment of condensation.

Despite the apparent complexity of the Gibbs function approach, with its implicit representation of the equation of state, the additional computational cost is rather modest. Calls to evaluate the Gibbs function and its derivatives are made $1 + 5N_{\text{Newton}}$ times per grid cell per step, where N_{Newton} is the number of Newton iterations. One call is needed to evaluate $\rho^{(w)}$ at time level n in (18). Then, for each Newton iteration, one call is needed to evaluate $\rho^{(w)}$ at time level $n+1$ in (18), two calls are needed to evaluate $1/c^2$, N^2, and the residuals in (9) and (10) at ρ-levels and w-levels, and two calls are needed for the back substitution to compute T' and $T^{(w)\prime}$. The number of calls could be reduced at the price of increased storage by saving some information rather than recomputing it.

The choice to use the Gibbs function rather than one of the other thermodynamic potentials deserves some discussion. Feistel *et al.* (2010) note that the Gibbs function is convenient because it expresses all properties as functions of p and T, which are directly measurable. Near a phase transition $g(p,T)$ and $h(p,\eta)$ are multivalued, so we must consider separate g or h for each phase and impose the condition for equilibrium to determine how much of each phase is present. On the other hand, $e(\alpha,\eta)$ and $f(\alpha,T)$ are single valued even near a phase transition, and so at first might appear more convenient. However, near a phase transition the sound speed squared can become negative at certain points in (α,η) or (α,T) space, and this could be problematic in a numerical model. Thus whichever thermodynamic potential is used, some special treatment will be needed near phase transitions. The Gibbs function is appealing for the treatment of phase equilibria because p and T are input arguments; thus two of the three criteria for equilibrium (equal p and equal T in the two phases) are automatically satisfied, and determining the equilibrium is then a problem in a single unknown.

In this paper sources and sinks of heat and water have been neglected, and equilibrium between liquid water and vapour has been assumed. In reality, sources, sinks, and departures from equilibrium, including fallout and evaporation of condensate, are important for many meteorological processes (e.g. Bannon 2002; Raymond 2013, and references therein), and their inclusion significantly complicates the governing equations. Nevertheless, a self-consistent equilibrium, source-free formulation should be a useful starting point for the inclusion of such processes.

In weather prediction and climate models important subgrid processes such as radiation, boundary layer fluxes, and shallow and deep convection are parameterized. In typical computer codes the equation of state appears implicitly or explicitly in numerous places, and adapting those parameterizations to make use of a Gibbs function would involve major effort. Nevertheless, it is hoped that the self-consistency of the Gibbs function approach, together with its flexibility to simplify, or 'upgrade', the equation of state will encourage model developers to consider the approach.

Acknowledgements

This work benefited from valuable discussions with Tommaso Benacchio, Geoffrey Vallis, Martin Willett, and Nigel Wood, as well as constructive reviews by Rupert Klein and an anonymous reviewer. It was funded in part by the Natural Environment Research Council under grant NE/N013123/1 as part of the ParaCon programme.

Appendix A. Some common thermodynamic quantities

This Appendix summarizes how some thermodynamic quantities commonly used in Meteorology can be expressed in terms of the Gibbs function and its derivatives. See Feistel *et al.* (2010) for more details and derivations, but note that they use a different definition of equivalent potential temperature.

Given p, T, and q, some quantities can be calculated directly from the derivatives of the Gibbs function:

- Specific heat capacity at constant pressure

$$C_p = -Tg_{TT}; \tag{70}$$

- specific heat capacity at constant volume

$$C_v = \frac{T\left(g_{pT}^2 - g_{pp}g_{TT}\right)}{g_{pp}}; \tag{71}$$

- specific enthalpy

$$h = g - Tg_T; \tag{72}$$

- specific internal energy

$$e = g - pg_p - Tg_T; \tag{73}$$

- latent heat of vaporization

$$\begin{aligned} L^v &= h^{av} - ah_a^{av} - h^l \\ &= g^{av} - ag_a^{av} - Tg_T^{av} + aTg_{Ta}^{av} \\ &- g^l + Tg_T^l; \end{aligned} \tag{74}$$

- inverse sound speed squared

$$\frac{1}{c^2} = \frac{g_{pT}^2 - g_{pp}g_{TT}}{g_p^2 g_{TT}}; \tag{75}$$

- static stability

$$\begin{aligned} N^2 &= -\Phi_z \left((\ln\rho)_\eta \Big|_{pq} \eta_z + (\ln\rho)_q \Big|_{\eta p} q_z \right) \\ &= -\Phi_z \rho \left\{ \left(\frac{g_{pT}}{g_{TT}} \right) \eta_z + \left(\frac{g_{pT}g_{Tq}}{g_{TT}} - g_{pq} \right) q_z \right\} \end{aligned} \tag{76}$$

Some quantities must be found by solving an implicit equation or system of equations for the desired quantity:

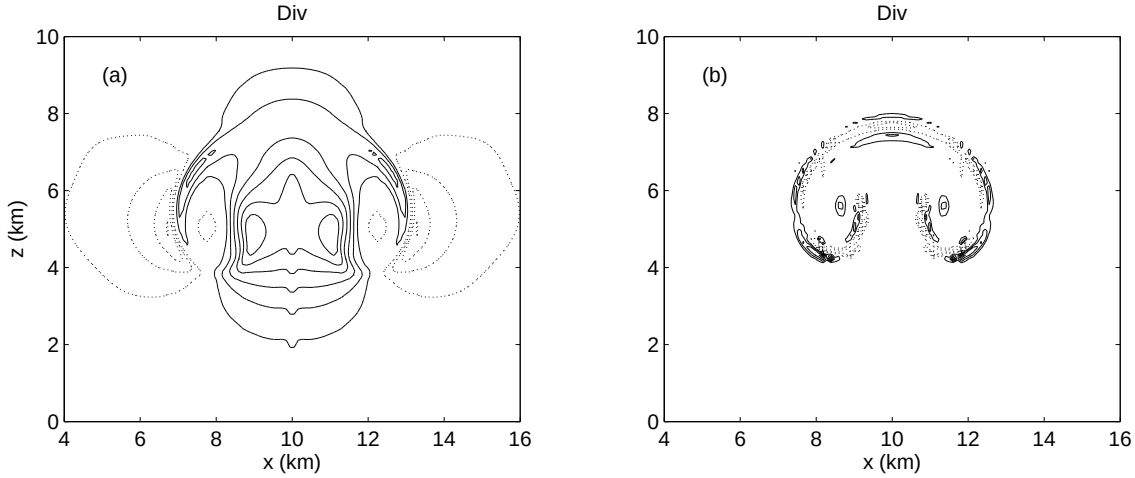

Figure 4. Divergence at $t = 1000\,\mathrm{s}$ for (a) dry air, contour interval $2 \times 10^{-4}\,\mathrm{s}^{-1}$, and (b) incompressible fluid, contour interval $2 \times 10^{-6}\,\mathrm{s}^{-1}$. Negative contours are dotted and the zero contour is omitted.

- Potential temperature

$$g_T\left(p_0, \theta, q\right) = g_T\left(p, T, q\right), \tag{77}$$

(in the pseudo-incompressible case the left hand side must be evaluated at $z = 0$ and the right hand side at the current height z);

- equivalent potential temperature

$$(1-q)g_T^{av}\left(p_0, \theta_e, a=1\right) + q g_T^{l}\left(p_0, \theta_e\right) = g_T\left(p, T, q\right); \tag{78}$$

- relative humidity

$$\mathcal{H} = \frac{p^v}{p^{\mathrm{sat}}} = \frac{(1-a)\left(1 + a_{\mathrm{sat}}(\varepsilon - 1)\right)}{(1-a_{\mathrm{sat}})\left(1 + a(\varepsilon - 1)\right)} \tag{79}$$

where

$$\mu^v\left(p, T, a_{\mathrm{sat}}\right) = \mu^l\left(p, T\right), \tag{80}$$

$$\mu^v = g^{av} - a g_a^{av}, \tag{81}$$

and

$$\mu^l = g^l; \tag{82}$$

- dewpoint temperature

$$\mu^v\left(p, T_d, a\right) = \mu^l\left(p, T_d\right); \tag{83}$$

- lifting condensation level (for a subsaturated parcel)

$$\left.\begin{array}{l} \mu^v\left(p_{\mathrm{LCL}}, T_{\mathrm{LCL}}, a\right) = \mu^l\left(p_{\mathrm{LCL}}, T_{\mathrm{LCL}}\right); \\ g_T\left(p_{\mathrm{LCL}}, T_{\mathrm{LCL}}, q\right) = g_T\left(p, T, q\right). \end{array}\right\} \tag{84}$$

For all of these quantities a small number of Newton iterations (around three) was found to give sufficient accuracy for practical purposes.

Appendix B. Derivatives of example Gibbs functions

The derivatives of the example Gibbs functions given in section 3 are listed here for the convenience of readers wishing to implement them in their own code.

7.1. *Dry air (section 3.1)*

$$g_p = \frac{R^d T}{p}; \qquad g_T = -C_p^d\left\{1 + \ln\left(\frac{T}{T_0}\right)\right\} + R^d \ln\left(\frac{p}{p_0^d}\right); \tag{85}$$

$$g_{pp} = -\frac{R^d T}{p^2}; \qquad g_{pT} = \frac{R^d}{p}; \qquad g_{TT} = -\frac{C_p^d}{T}. \tag{86}$$

7.2. *Air and water vapour (section 3.2)*

The derivatives of g^{av} are given by

$$g_p^{av} = \left(aR^d + (1-a)R^v\right)\frac{T}{p}; \tag{87}$$

$$\begin{aligned} g_T^{av} = & -\left(aC_p^d + (1-a)C_p^v\right)\left\{1 + \ln\left(\frac{T}{T_0}\right)\right\} \\ & + \left(aR^d L^{(1)} + (1-a)R^v L^{(2)}\right) \\ & - (1-a)\frac{L_0^v}{T_0}; \end{aligned} \tag{88}$$

$$\begin{aligned} g_a^{av} = & -\left(C_p^d - C_p^v\right) T \ln\left(\frac{T}{T_0}\right) \\ & + \left\{R^d\left(aL^{(1)}\right)_a + R^v\left((1-a)L^{(2)}\right)_a\right\} T \\ & - L_0^v\left(1 - \frac{T}{T_0}\right); \end{aligned} \tag{89}$$

and

$$g_{pp}^{av} = -\left(aR^d + (1-a)R^v\right)\frac{T}{p^2}; \tag{90}$$

$$g_{pT}^{av} = \left(aR^d + (1-a)R^v\right)\frac{1}{p}; \tag{91}$$

$$g_{TT}^{av} = -\left(aC_p^d + (1-a)C_p^v\right)\frac{1}{T}; \tag{92}$$

$$g_{pa}^{av} = \left(R^d - R^v\right)\frac{T}{p}; \tag{93}$$

$$\begin{aligned} g_{Ta}^{av} = & -\left(C_p^d - C_p^v\right)\left\{1 + \ln\left(\frac{T}{T_0}\right)\right\} \\ & + \left\{R^d\left(aL^{(1)}\right)_a + R^v\left((1-a)L^{(2)}\right)_a\right\} \\ & + \frac{L_0^v}{T_0}; \end{aligned} \tag{94}$$

$$g_{aa}^{av} = \left\{R^d\left(aL^{(1)}\right)_{aa} + R^v\left((1-a)L^{(2)}\right)_{aa}\right\} T. \tag{95}$$

These expressions may be evaluated making use of

$$\left(aL^{(1)}\right)_a = L^{(1)} + \frac{1}{(1 + a(\varepsilon - 1))}; \tag{96}$$

$$\left(aL^{(1)}\right)_{aa} = \frac{1}{a\left(1 + a(\varepsilon - 1)\right)^2}; \tag{97}$$

$$\left((1-a)L^{(2)}\right)_a = -L^{(2)} - \frac{\varepsilon}{(1 + a(\varepsilon - 1))}; \tag{98}$$

$$\left((1-a)L^{(2)}\right)_{aa} = \frac{\varepsilon^2}{(1-a)\left(1 + a(\varepsilon - 1)\right)^2}. \tag{99}$$

(100)

Note that g^{av}_{Ta} and g^{av}_{aa} blow up in the limits $a \to 1$ (pure air) and $a \to 0$ (pure water vapour); in these limits it is safest to use $g^{av} = g^a$ and $g^{av} = g^v$, respectively.

7.3. *Liquid water (section 3.2)*

The derivatives of g^l are given by

$$
\begin{aligned}
g^l_p &= \alpha^l; && (101)\\
g^l_T &= -C^l \left\{ 1 + \ln\left(\frac{T}{T_0}\right)\right\} - \frac{\alpha^l p_0^{\rm sat}}{T_0}; && (102)\\
g^l_{pp} &= 0; && (103)\\
g^l_{pT} &= 0; && (104)\\
g^l_{TT} &= -\frac{C^l}{T}. && (105)\\
& && (106)
\end{aligned}
$$

7.4. *Humid and wet air (section 3.2)*

If $a > a_{\rm sat}$ then the air is unsaturated and

$$
\begin{aligned}
g_q &= -g^{av}_a, & g_{pq} &= -g^{av}_{pa},\\
g_{Tq} &= -g^{av}_{Tq}, & g_{qq} &= g^{av}_{aa}, && (107)
\end{aligned}
$$

with the other partial derivatives of g equal to the corresponding partial derivatives of g^{av}.

In the saturated case care is needed in calculating the partial derivatives of g since we must allow for changes in the fractions of vapour and liquid water, noting that the equilibrium $\mu^v = \mu^l$ must be maintained. Also, attention must be paid to what is held constant (q or a) as derivatives with respect to p and T are taken. After some manipulation we obtain (Feistel *et al.* 2010)

$$
\begin{aligned}
g_p &= (1-q^l) g^{av}_p + q^l g^l_p, && (108)\\
g_T &= (1-q^l) g^{av}_T + q^l g^l_T, && (109)\\
g_q &= \left(g^l - g^{av}\right)/a, && (110)\\
g_{pp} &= (1-q^l) g^{av}_{pp} + q^l g^l_{pp} - (1-q^l)\frac{\Lambda_p^2}{a^2 g^{av}_{aa}}, && (111)\\
g_{pT} &= (1-q^l) g^{av}_{pT} + q^l g^l_{pT} - (1-q^l)\frac{\Lambda_p \Lambda_T}{a^2 g^{av}_{aa}}, && (112)\\
g_{TT} &= (1-q^l) g^{av}_{TT} + q^l g^l_{TT} - (1-q^l)\frac{\Lambda_T^2}{a^2 g^{av}_{aa}}, && (113)\\
g_{pq} &= \left(g^l_p - g^{av}_p\right)/a, && (114)\\
g_{Tq} &= \left(g^l_T - g^{av}_T\right)/a, && (115)\\
g_{qq} &= 0, && (116)
\end{aligned}
$$

where

$$
\begin{aligned}
\Lambda_p &= g^{av}_p - a g^{av}_{pa} - g^l_p, && (117)\\
\Lambda_T &= g^{av}_T - a g^{av}_{Ta} - g^l_T. && (118)
\end{aligned}
$$

7.5. *Pseudo-incompressible (section 3.3)*

The derivatives of g are

$$
\begin{aligned}
g_p &= \frac{R^d T}{(1-\kappa)p_r + \kappa p}, && (119)\\
g_T &= C^d_p \left[\ln\left\{ \Pi_r \left((1-\kappa) + \kappa \frac{p}{p_r}\right)\right\} \right.\\
&\quad \left. - \left\{ 1 + \ln\left(\frac{T}{T_0}\right)\right\}\right], && (120)\\
g_{pp} &= -\frac{\kappa R^d T}{\left((1-\kappa)p_r + \kappa p\right)^2}, && (121)\\
g_{pT} &= \frac{R^d}{(1-\kappa)p_r + \kappa p}, && (122)\\
g_{TT} &= -\frac{C^d_p}{T}. && (123)
\end{aligned}
$$

7.6. *Incompressible (section 3.4)*

The derivatives of g are

$$
\begin{aligned}
g_p &= \frac{R^d T}{(1-\kappa)p^d_0 + \kappa p}, && (124)\\
g_T &= C^d_p \left[\ln\left((1-\kappa) + \kappa \frac{p}{p^d_0}\right) - \left\{ 1 + \ln\left(\frac{T}{T_0}\right)\right\}\right], && (125)\\
g_{pp} &= -\frac{\kappa R^d T}{\left((1-\kappa)p^d_0 + \kappa p\right)^2}, && (126)\\
g_{pT} &= \frac{R^d}{(1-\kappa)p^d_0 + \kappa p}, && (127)\\
g_{TT} &= -\frac{C^d_p}{T}. && (128)
\end{aligned}
$$

References

Akmaev RA. 2011. Whole atmosphere modeling: Connecting terrestrial and space weather. *Rev. Geophys.* **49**(RG4004), doi:10.1029/2011/RG000364.

Bannon PR. 2002. Theoretical foundations for models of moist convection. *J. Atmos. Sci.* **59**: 1967–1982.

Benacchio T, O'Neill WP, Klein R. 2014. A blended soundproof-to-compressible numerical model for small- to mesoscale atmospheric dynamics. *Mon. Wea. Rev.* **142**: 4416–4438.

Bolton D. 1980. The computation of equivalent potential temperature. *Mon. Wea. Rev.* **108**: 1046–1053.

Bryan GH, Fritsch JM. 2002. A benchmark simulation for moist nonhydrostatic numerical models. *Mon. Wea. Rev.* **130**: 2917–2928.

Curry JA, Webster PJ. 1999. *Thermodynamics of Atmospheres and Oceans*. Academic Press.

Davies T, Cullen MJP, Malcolm AJ, Mawson MH, Staniforth A, White AA, Wood N. 2005. A new dynamical core for the Met Office's global and regional modelling of the atmosphere. *Quart. J. Roy. Meteor. Soc.* **131**: 1759–1782.

Durran DR. 1989. Improving the anelastic approximation. *J. Atmos. Sci.* **46**: 1453–1461.

Emanuel KA. 1994. *Atmospheric Convection*. Oxford University Press.

Feistel R, Wright DG, Kretzschmar HJ, Hagen E, Herrmann S, Span R. 2010. Thermodynamic properties of sea air. *Ocean Sci.* **6**: 91–141.

IOC, SCOR, IAPSO. 2010. The international thermodynamic equation of seawater–2010: Calculation and use of thermodynamic properties. Intergovernmental Oceanographic Commission, Manuals and Guides No. 56, URL http://www.TEOS-10.org.

Klein R, Benacchio T. 2016. A doubly blended model for multiscale atmospheric dynamics. *J. Atmos. Sci.* **73**: 1179–1186.

Klein R, Pauluis O. 2012. Thermodynamic consistency of a pseudoincompressible approximation for general equations of state. *J. Atmos. Sci.* **69**: 961–968.

Kurowski MJ, Grabowski WW, Smolarkiewicz PK. 2014. Anelastic and compressible simulations of moist deep convection. *J. Atmos. Sci.* **71**: 3767–3787.

Melvin T, Dubal M, Wood N, Staniforth A, Zerroukat M. 2010. An inherently mass-conserving iterative semi-implicit semi-Lagrangian discretization of the non-hydrostatic vertical-slice equations. *Quart. J. Roy. Meteor. Soc.* **136**: 799–814.

Militzer B, Hubbard WB. 2013. Ab initio equation of state for hydrogen-helium mixtures with recalibration of the giant-planet mass-radius relation. *Astrophys. J.* **774**(148), doi:10.1088/0004-637X/774/2/148.

Raymond DJ. 2013. Sources and sinks of entropy in the atmosphere. *J. Adv. Modeling Earth Sys.* **5**: 755–763.

Read PL, Thomas NPJ, Risch SH. 2000. An evaluation of Eulerian and semi-Lagrangian advection schemes in simulations of rotating, stratified flows in the laboratory. Part I: Axisymmetric flow. *Mon. Wea. Rev.* **128**: 2835–2852.

Smolarkiewicz PK, Kuehnlein C, Wedi NP. 2014. A consistent framework for discrete integrations of soundproof and compressible pdes of atmospheric dynamics. *J. Comput. Phys.* **263**: 185–205.

Staniforth A. 2014. Deriving consistent approximate models of the global atmosphere using Hamilton's principle. *Quart. J. Roy. Meteor. Soc.* **140**: 2383–2387.

Thuburn J. 2017. Vertical discretizations giving optimal representation of normal modes: General equations of state. To appear in Quart. J. Roy. Meteorol. Soc.

Thuburn J, Zerroukat M, Wood N, Staniforth A. 2010. Coupling a mass-conserving semi-Lagrangian scheme (SLICE) to a semi-implicit discretisation of the shallow-water equations: Minimizing the dependence on a reference atmosphere. *Quart. J. Roy. Meteor. Soc.* **136**: 146–154.

Tort M, Dubos T. 2014. Usual approximations to the equations of atmospheric motion: a variational perspective. *J. Atmos. Sci.* **71**: 2452–2466.

Vallis GK. 2006. *Atmospheric and Oceanic Fluid Dynamics*. Cambridge University Press.

Wood N, Staniforth A, White A, Allen T, Diamantakis M, Gross M, Melvin T, Smith C, Vosper S, Zerroukat M, Thuburn J. 2014. An inherently mass-conserving semi-implicit semi-lagrangian discretisation of the deep-atmosphere global nonhydrostatic equations. *Quart. J. Roy. Meteor. Soc.* **140**: 1505–1520, doi:10.1002/qj.2235.

Zerroukat M, Wood N, Staniforth A. 2009. An improved version of SLICE for conservative monotonic remapping on a C-grid. *Quart. J. Roy. Meteor. Soc.* **135**: 541–546.

